

Supporting Information

Trace F-doped Co_3O_4 nanoneedles for enhanced acidic water oxidation activity via promoting OH coverage

Genyan Hao^{a,#}, Tao Zhao^{b,c,#}, Qiang Fang^{b,c,#}, Yunzhen Jia^{b,c}, Dandan Li^d, Dazhong

Zhong^{b,c,*}, Jinping Li^{b,c}, Qiang Zhao^{b,c,*}

^a Shanxi College of Technology, Shuozhou 036000, Shanxi, P.R. China.

^b College of Chemical Engineering and Technology, Taiyuan University of
Technology, Taiyuan 030024, Shanxi, P.R. China.

^c Shanxi Key Laboratory of Gas Energy Efficient and Clean Utilization, Taiyuan
030024, Shanxi, P.R. China.

^d Shandong Provincial Key Laboratory of Chemical Energy Storage and Novel Cell
Technology, School of Chemistry and Chemical Engineering, Liaocheng University,
Liaocheng 252059, Shandong, P.R. China.

These authors contributed equally to this work.

*Corresponding authors.

E-mail addresses: zhaoqiang@tyut.edu.cn (Q. Zhao); zhongdazhong@tyut.edu.cn
(D.Z. Zhong).

1. Membrane electrode assembly (MEA) testing

F-Co₃O₄/CP (IrO₂/CP) and commercial Pt/C/CP were used as anode and cathode for water splitting test, respectively (0.5 M H₂SO₄ and 25 °C). In addition, F-Co₃O₄/CP and commercial Ag NPs were used as anode and cathode for CO₂RR test, respectively (0.5 M H₂SO₄ and 25 °C). Anion exchange membranes (117) were used to separate the side of the anode and cathode.

2. Calculation methods

The Vienna ab initio simulation package (VASP) were used for spin-polarized and periodic density function theory (DFT) calculations. Exchange-correlation was treated within the generalized approximation of Perdew-Burke-Ernzerhof (GGA-PBE). A cutoff energy was set as 450 eV to ensure accurate energies with errors of less than 1 meV per atom. The self-consistency of the electron which defined by energy threshold established as 10⁻⁴ eV, whereas geometry optimization was converged when the forces with energy change were lower than 0.05 eV/Å. At the same time, the Co₃O₄ (311) model and 15 Å vacuum layer which make sure that there is no interaction between adjacent images were built by Materials Studio. And the discussion of frequency analysis and zero-point vibrational energies (ZPE) is used by VASPKIT for thermodynamic corrections and stability discussions of intermediate adsorption. A 5×5×5 Monkhorst-Pack k-point grid was used for the optimization of the unit structure, determined by minimizing the general energy of the unit cell by means of conjugated gradient algorithm. In addition, the corrections of Hubbard term (PBE+U) and dispersion (DFT+D3) was tested on account of the gradient approximation (GGA)

functional underrate the energy of the 4d orbital and the band gap of the homologous material. To describe this effect, U_{eff} was set as 4 eV for Co-3d, and a $2\times 2\times 1$ Monkhorst-Pack k-point grids was used for the optimization of Co_3O_4 (311) surface model and adsorption process of DFT calculations, while $4\times 4\times 1$ for density of states (DOS) and differential charge calculations.

The electron reaction paths of oxygen evolution reaction (OER) in our DFT calculation follows the process below:



The Gibbs free energy (ΔG) of each oxygen evolution reaction steps is calculated by the following formula:

$$\Delta G = \Delta E_{DFT} + \Delta ZPE - T\Delta S - eU$$

Where ΔE_{DFT} , ΔZPE , ΔS are the change of DFT total energy, zero-point energy, and entropy from the initial to the final state; U is the electrode potential and e is the transferred charge in the reaction.

The adsorption energies of ${}^*\text{OH}$, ${}^*\text{O}$ and ${}^*\text{OOH}$ are calculated by their DFT energy:

$$\Delta E_{ads} = E({}^*\text{OH}) - E_{slab} - E(\text{OH})$$

Where E_{slab} and $E(\text{OH})$ are considered as the DFT calculated energy for pure slab and the DFT energy for small molecules, respectively.

3. Calculation C_{dl}

C_{dl} : multi-turn CV curves were acquired at scan rates from 100 to 500 mV s⁻¹ in the non-Faradaic region (0.4 - 0.5 V vs. Hg/Hg₂SO₄), then the slope was obtained from a linear plot of the capacitive currents ($(\Delta j = j_{anodic} - j_{cathodic})/2$) versus scan rate, and the obtained slope was the C_{dl} value ¹.

4. Calculation ECSA

ECSA: the ECSA was obtained according to the formula: C_{dl}/C_s , where C_s indicates the specific capacitance and is 0.06 mF cm⁻² in H₂SO₄ ².

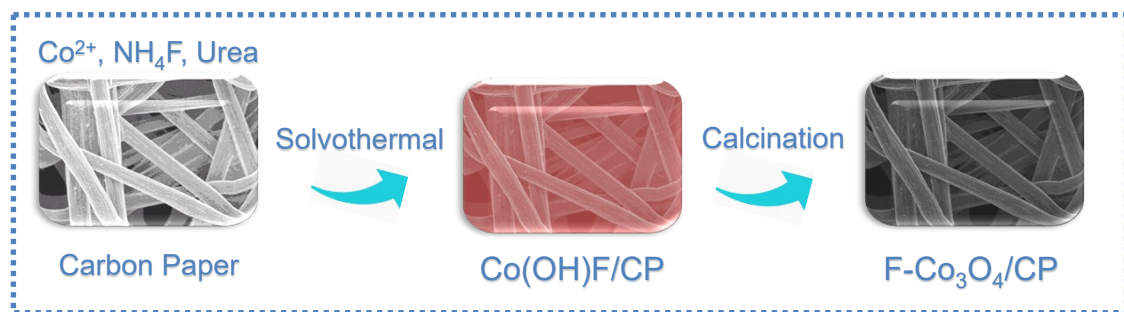


Fig. S1. Schematic illustration of $\text{F}-\text{Co}_3\text{O}_4/\text{CP}$ ($3 \text{ cm} \times 5 \text{ cm}$).

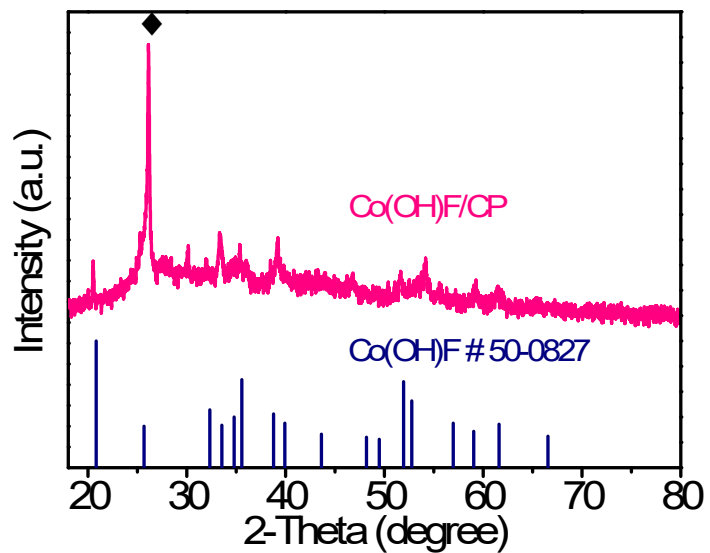


Fig. S2. XRD patterns of Co(OH)F/CP (26 ° belongs to CP peak).

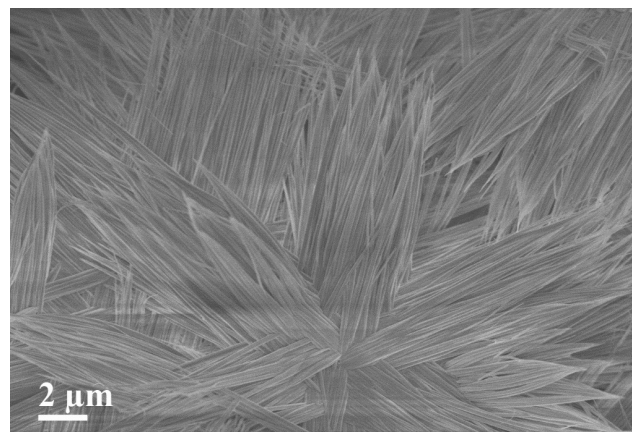


Fig. S3. SEM image of Co(OH)F/CP.

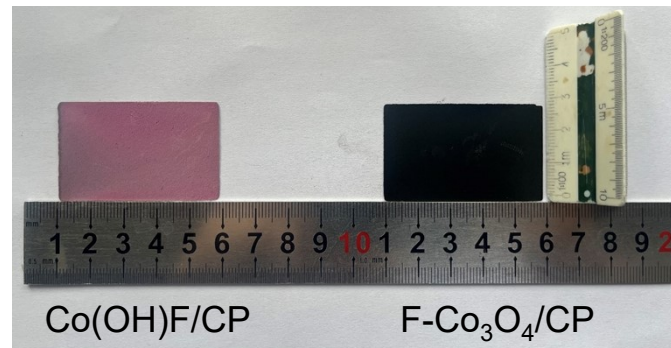


Fig. S4. Optical images of Co(OH)F/CP and F-Co₃O₄/CP (3 cm × 5 cm).

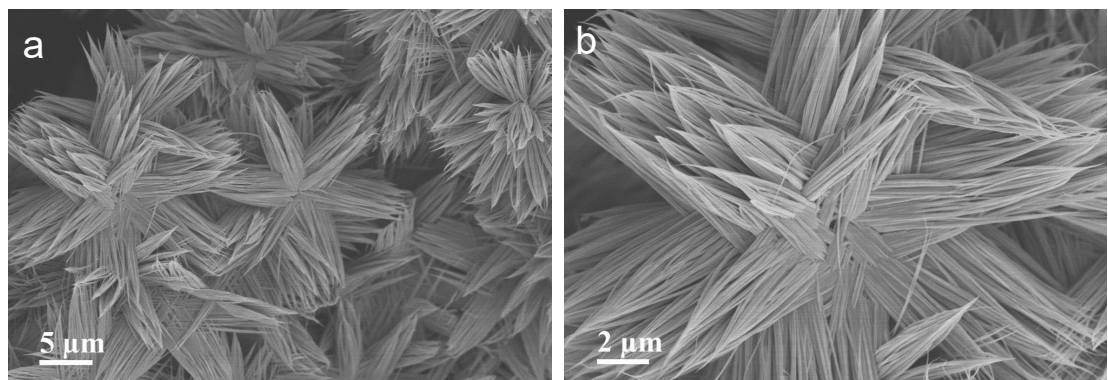


Fig. S5. SEM images of F-Co₃O₄/CP.

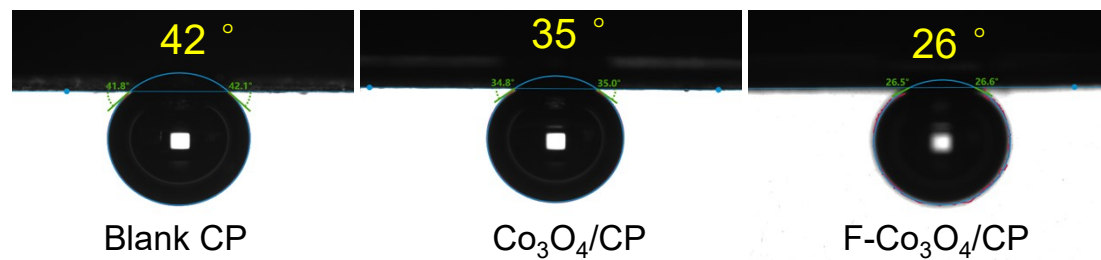


Fig. S6. CA of Blank CP, $\text{Co}_3\text{O}_4/\text{CP}$ and $\text{F}-\text{Co}_3\text{O}_4/\text{CP}$.

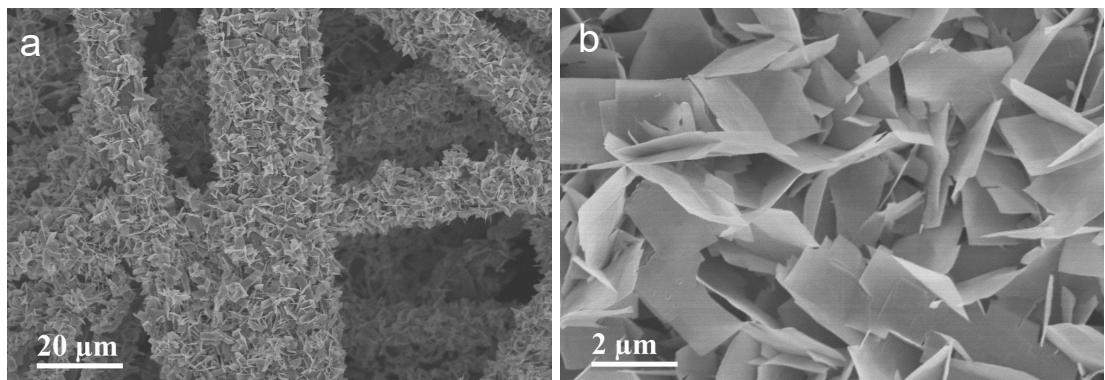


Fig. S7. SEM images of $\text{Co}_3\text{O}_4/\text{CP}$.

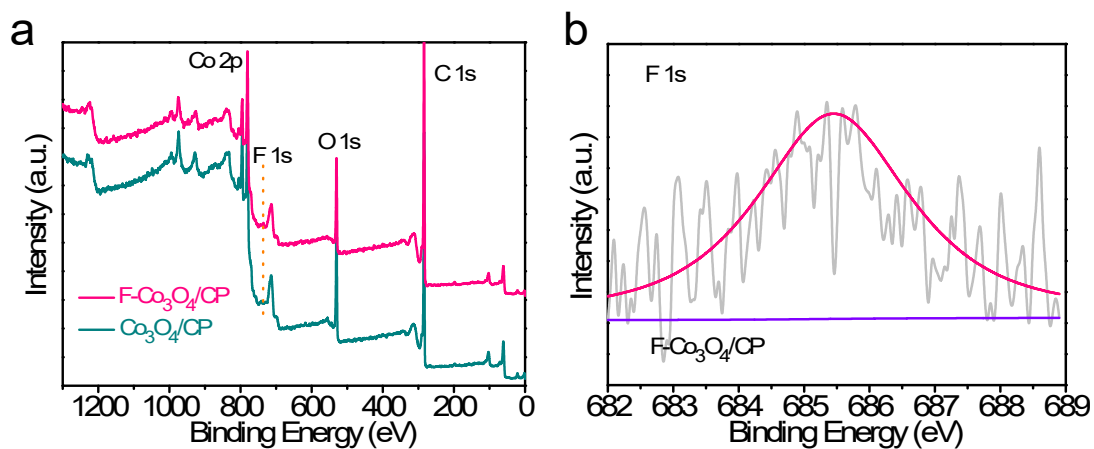


Fig. S8. (a) Fully measured XPS spectra of F-Co₃O₄/CP and Co₃O₄/CP, (b) F 1s XPS spectra of F-Co₃O₄/CP.

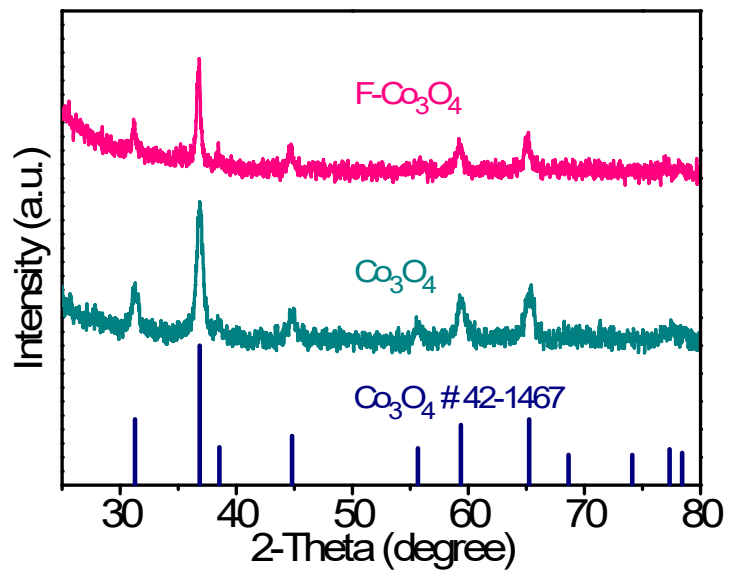


Fig. S9. XRD patterns of Co_3O_4 powder and F- Co_3O_4 powder.

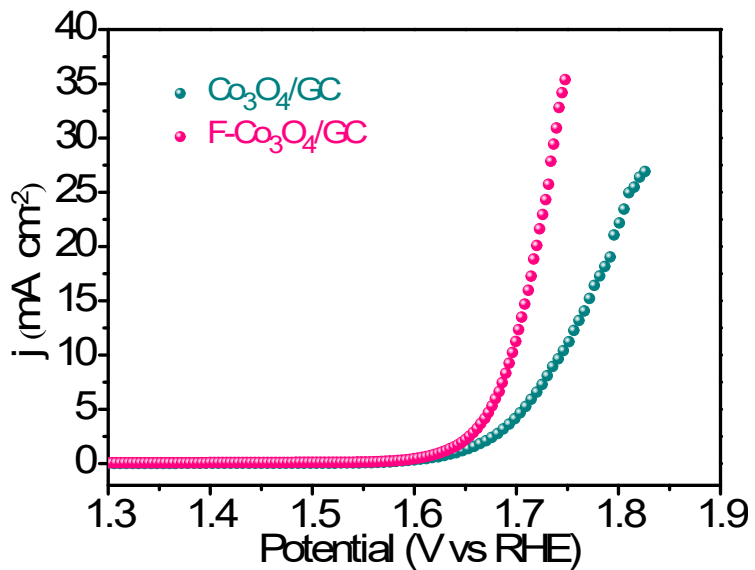


Fig. S10. LSV curves of Co₃O₄ powder and F-Co₃O₄ powder on GC.

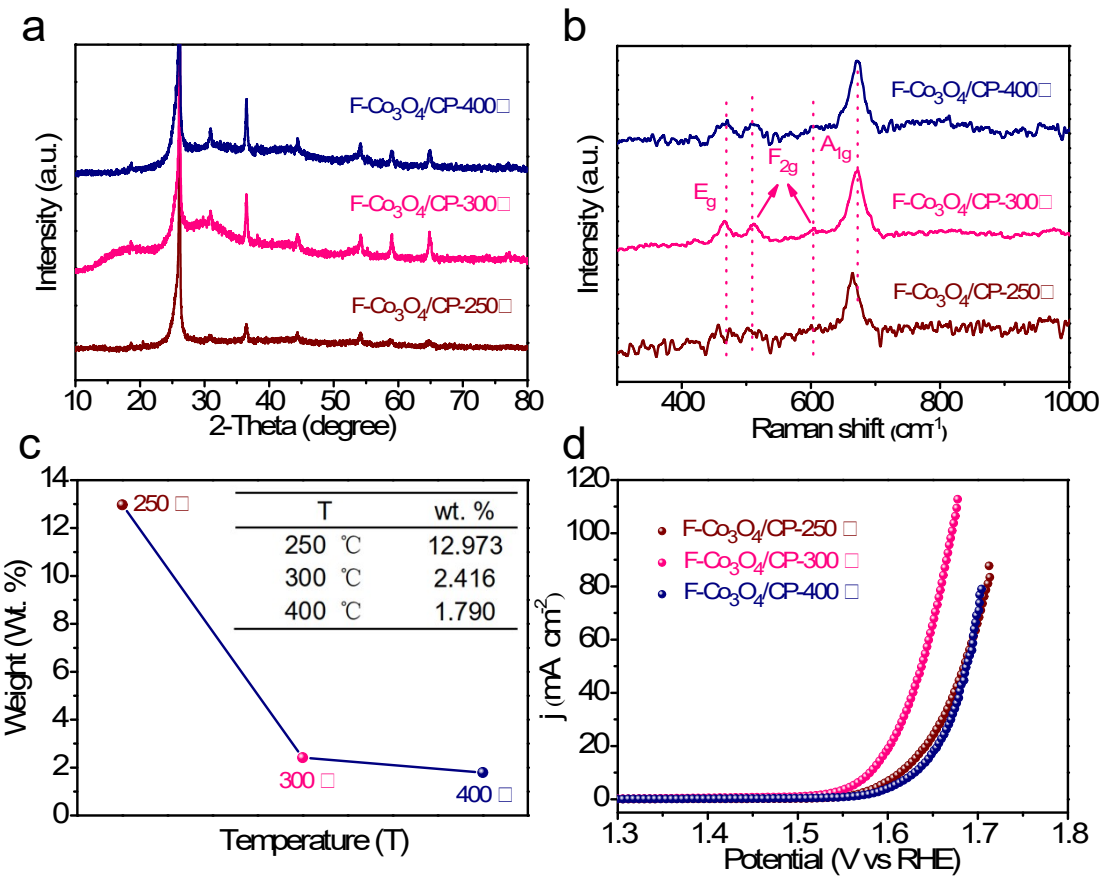


Fig. S11. (a) XRD patterns, (b) Raman spectra, (c) EDS data, (b) LSV curves for F-Co₃O₄/CP with different calcination temperatures.

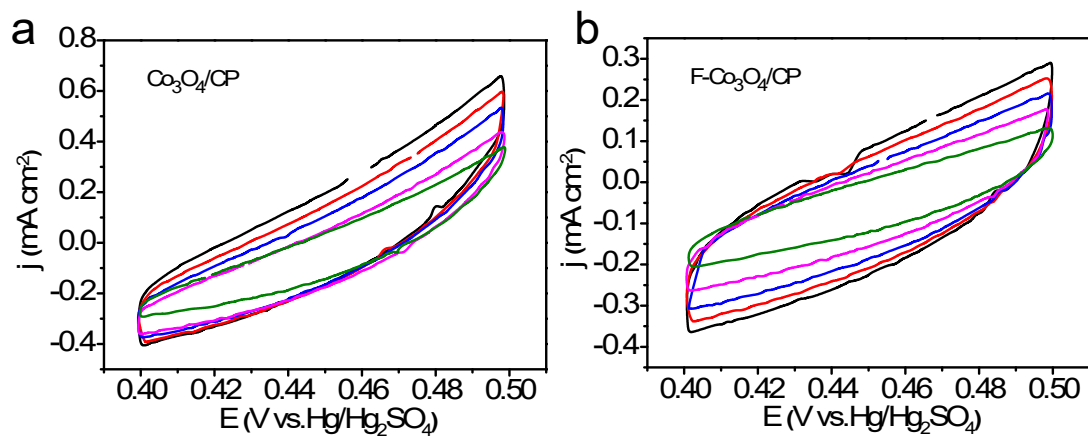


Fig. S12. CV curves at various scan rates (100, 200, 300, 400 and 500 mV s^{-1}) in the potential range of 0.40 – 0.50 V vs $\text{Hg/Hg}_2\text{SO}_4$ for $\text{Co}_3\text{O}_4/\text{CP}$ and $\text{F-Co}_3\text{O}_4/\text{CP}$.

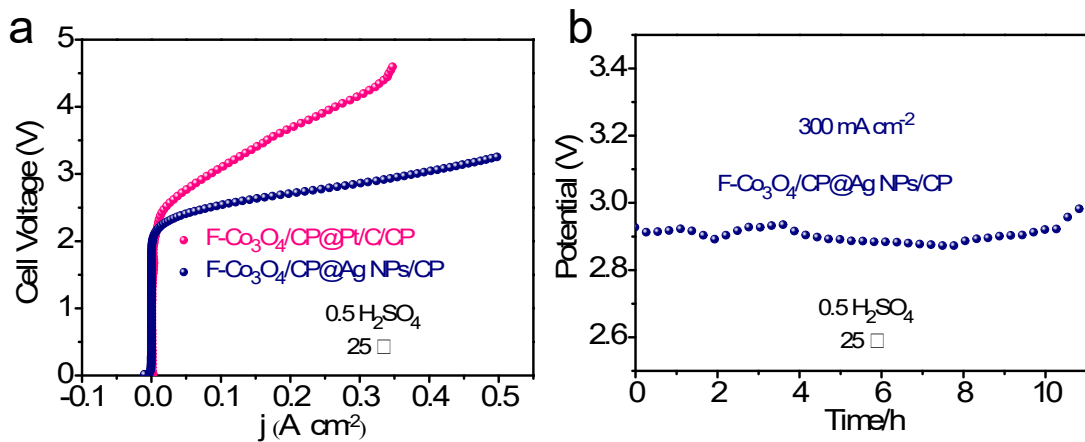


Fig. S13. (a) Polarization curves of the MEA using Pt/C/CP (Ag NPs/CP) for the HER (CO₂RR) and F-Co₃O₄/CP for the OER (0.5 M H₂SO₄ and 25 °C); (b) stability test at 300 mA cm⁻² (0.5 M H₂SO₄ and 25 °C).

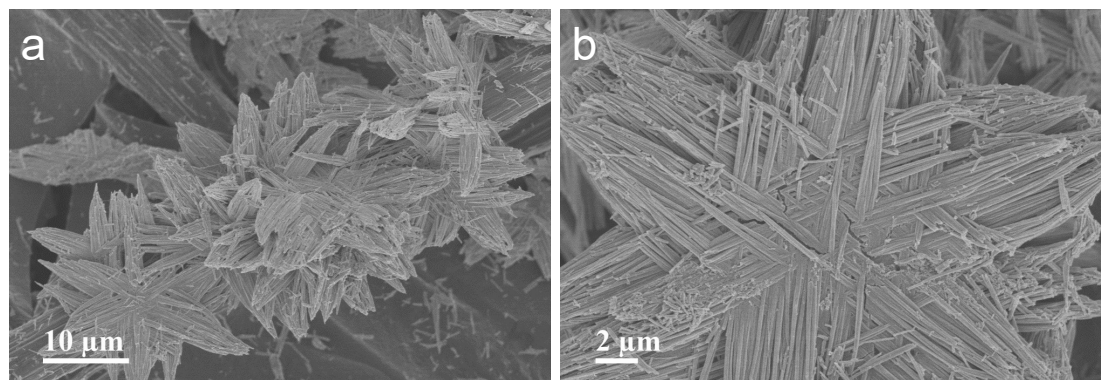


Fig. S14. SEM images of F-Co₃O₄/CP after OER.

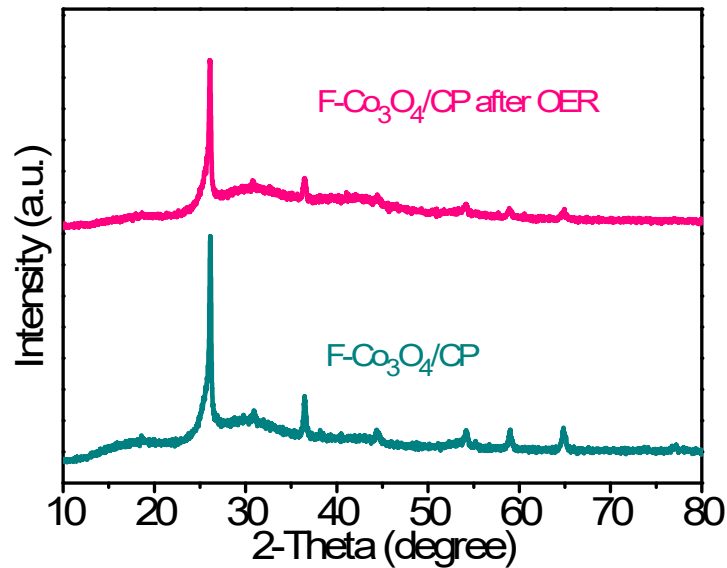


Fig. S15. XRD patterns of F-Co₃O₄/CP after OER.

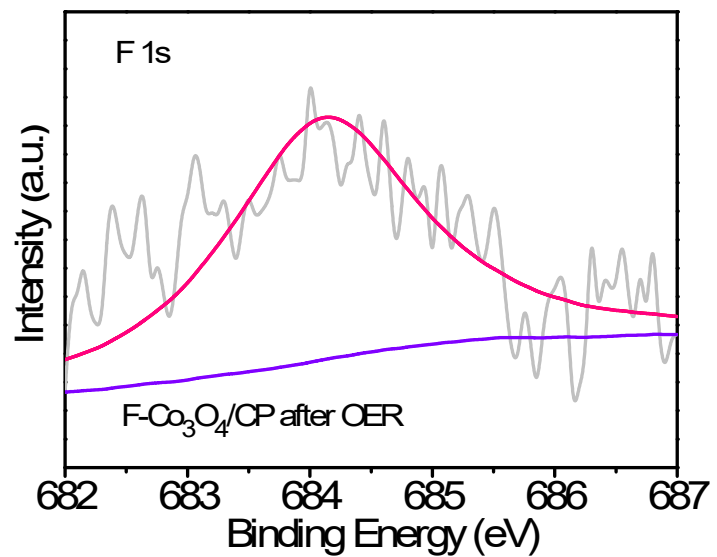


Fig. S16. F 1s XPS spectra of F-Co₃O₄/CP after OER.

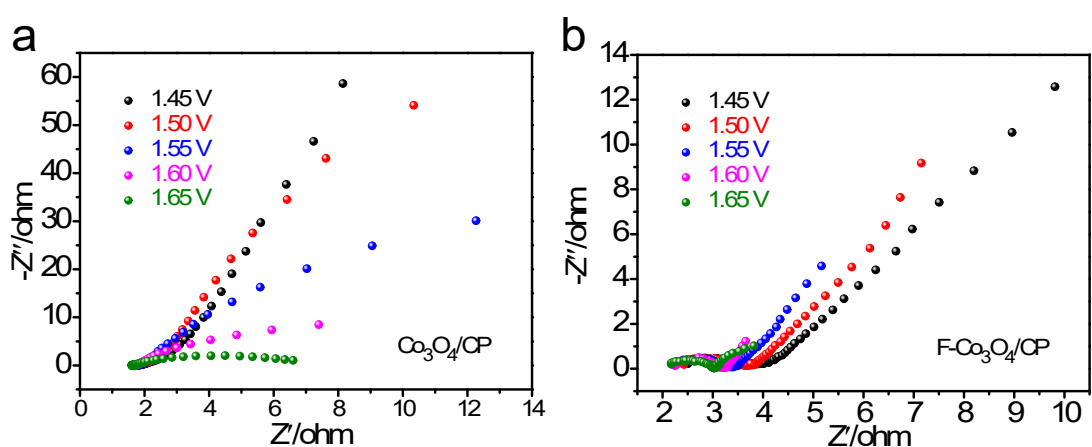


Fig. S17. EIS plots for $\text{Co}_3\text{O}_4/\text{CP}$ and $\text{F}-\text{Co}_3\text{O}_4/\text{CP}$ at various electrochemical potentials.

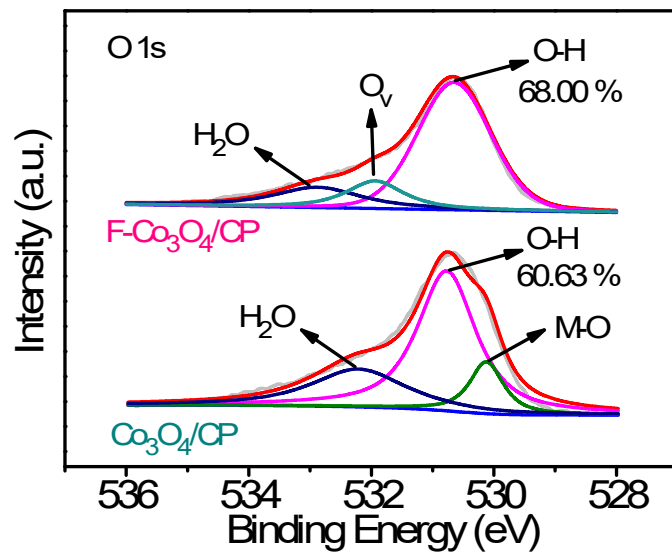


Fig. S18. O 1s XPS spectra of F-Co₃O₄/CP and Co₃O₄/CP.

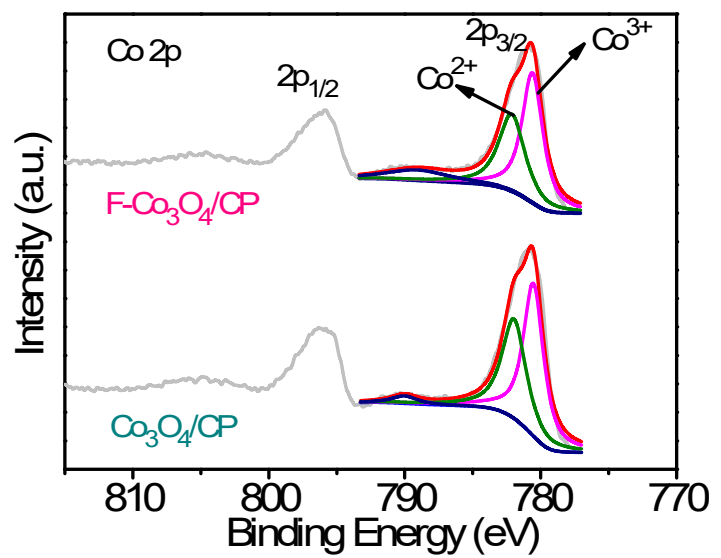


Fig. S19. Co 2p XPS spectra of F-Co₃O₄/CP and Co₃O₄/CP.

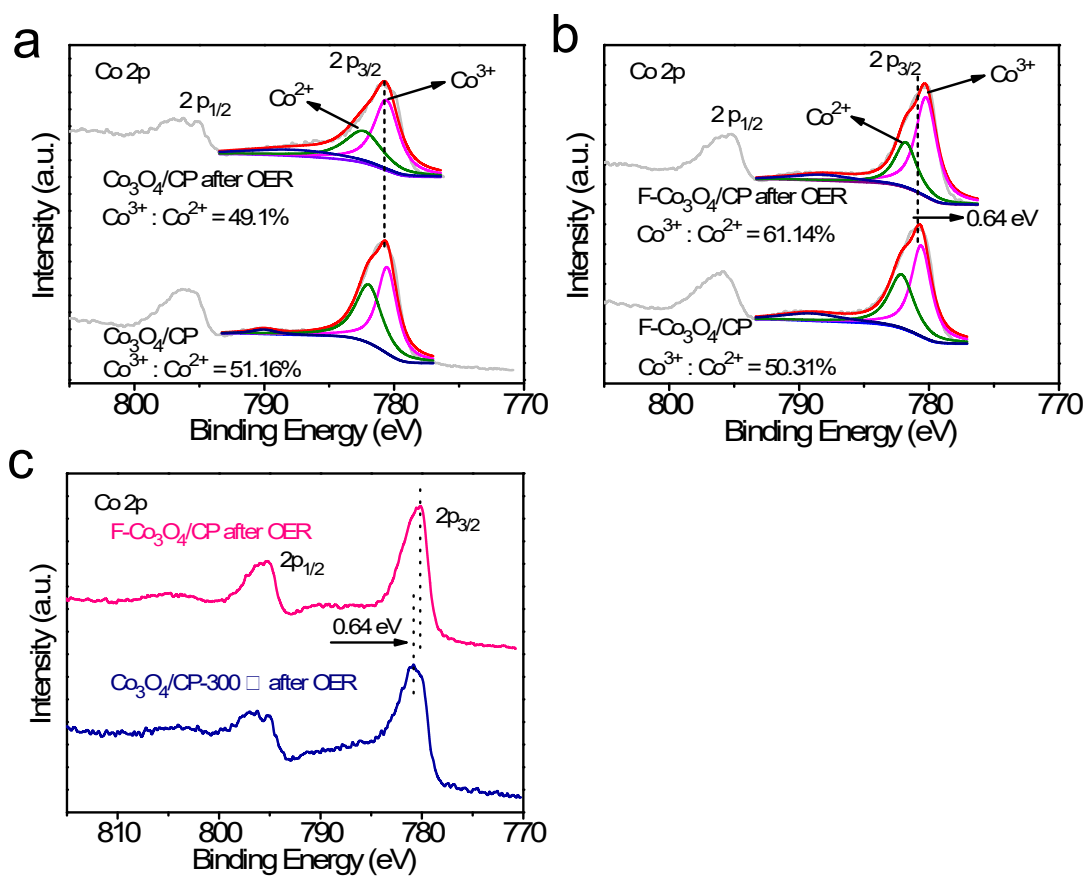


Fig. S20. Co 2p XPS spectra of F-Co₃O₄/CP, Co₃O₄/CP, F-Co₃O₄/CP after OER and Co₃O₄/CP after OER.

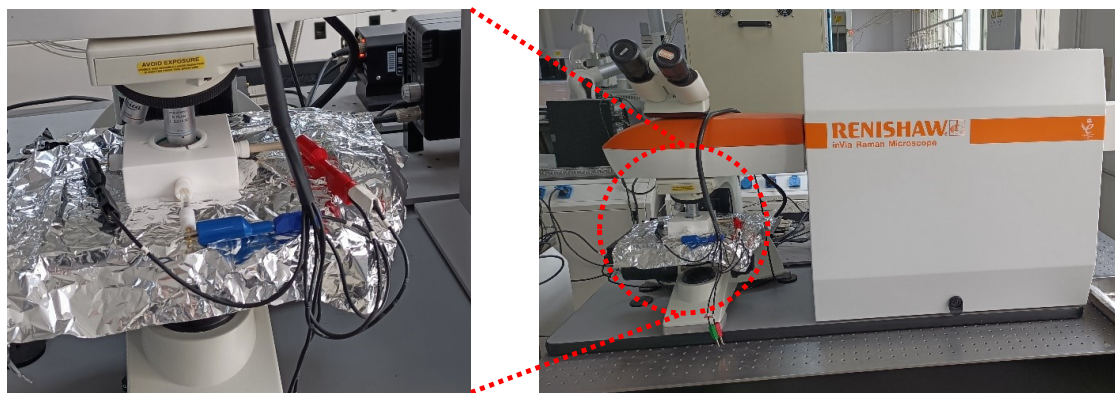


Fig. S21. Operando Raman system.

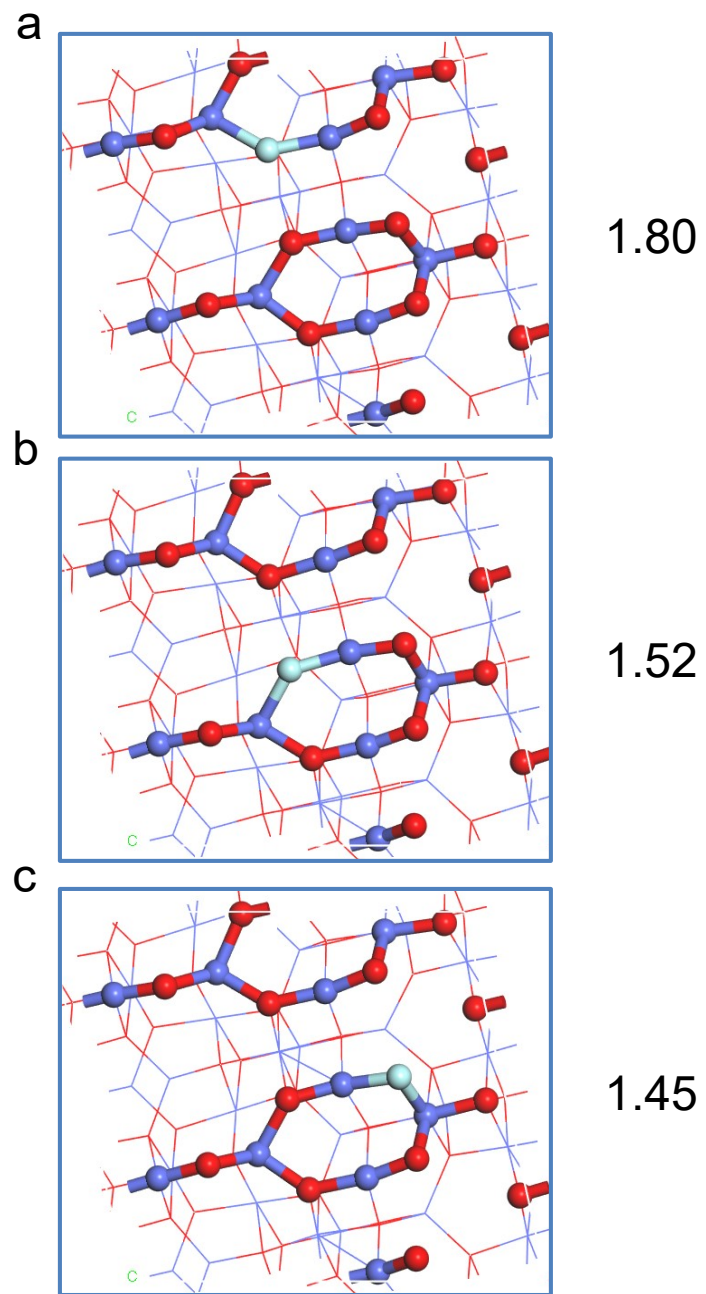


Fig. S22. The different substitution positions of F in Co_3O_4 (311) (Formation energy), where c is the optimal replacement for F(the atomic ratio of F and O is 1:13).

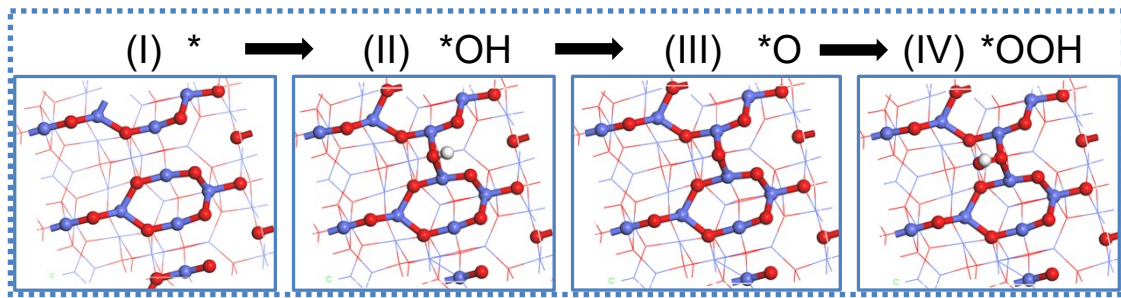


Fig. S23. Schematic representation of OER process for $\text{Co}_3\text{O}_4/\text{CP}$.

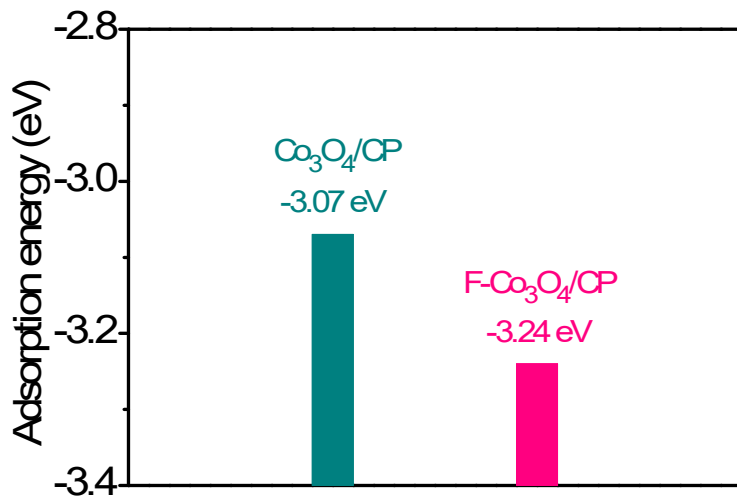


Fig. S24. Adsorption energies of OH on $\text{Co}_3\text{O}_4/\text{CP}$ and $\text{F}-\text{Co}_3\text{O}_4/\text{CP}$.

Table S1. Optimum fit parameters of the EIS data for Co₃O₄/CP (0.5 M H₂SO₄) (R₁: solution resistance; R₂/R_{ct}: electrochemical resistance; CPE₁: low frequency; CPE₂: high frequency).

Potential (vs RHE)	R ₁ (Ω)	R ₂ /R _{ct} (Ω)	R ₃ (Ω)	CPE ₁ (mF)	CPE ₂ (mF)
1.45 V	1.869	2.985	315.90	0.02037	0.03086
1.50 V	1.750	2.039	257.30	0.02063	0.03428
1.55 V	1.746	1.631	81.92	0.03837	0.05313
1.60 V	1.704	0.929	15.45	0.11480	0.15090
1.65 V	1.663	0.899	3.70	0.06514	0.10800

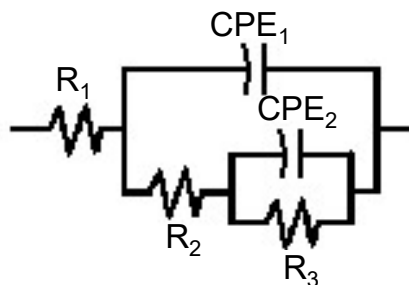


Table S2. Optimum fit parameters of the EIS data for F-Co₃O₄/CP (0.5 M H₂SO₄) (R₁: solution resistance; R₂/R_{ct}: electrochemical resistance; CPE₁: low frequency; CPE₂: high frequency).

Potential (vs RHE)	R ₁ (Ω)	R ₂ /R _{ct} (Ω)	R ₃ (Ω)	CPE ₁ (mF)	CPE ₂ (mF)
1.45 V	2.719	1.414	1808	0.00004	0.15190
1.50 V	2.533	1.304	14.54	0.00003	0.21820
1.55 V	2.299	1.141	7.83	0.00243	0.47840
1.60 V	2.264	0.943	2.21	0.94260	1.91900
1.65 V	2.164	0.857	1.69	21.09000	1.71700

Table S3. Comparison OER performance with other reported transition metal electrocatalysts in acidic media (0.5 M H₂SO₄).

Materials	Electrolytes	$\eta@10 \text{ mA cm}^{-2}$ (mV)	Reference s
F-Co ₃ O ₄	0.5 M H ₂ SO ₄	350 mV	This work
LMCF	0.5 M H ₂ SO ₄	353 mV	3
Co ₃ O ₄ /CeO ₂	0.5 M H ₂ SO ₄	423 mV	4
P-Co ₃ O ₄	0.5 M H ₂ SO ₄	400 mV	5
Co ₃ O ₄	0.5 M H ₂ SO ₄	570 mV	6
Ni ₂ Ta	0.5 M H ₂ SO ₄	570 mV	7
Ni _{0.5} Mn _{0.5} Sb _{1.7} O _y	1.0 M H ₂ SO ₄	670 mV	8
NiFeP	0.05 M H ₂ SO ₄	540 mV	9
FeN ₄ -CNF	0.5 M H ₂ SO ₄	294 mV	10
PbO ₂ /Co ₃ O ₄	1.0 M HClO ₄	460 mV	11
Cu _{1.5} Mn _{1.5} O ₄ :10F	0.5 M H ₂ SO ₄	325 mV	12
Mn _{0.67} Sb _{0.33} O ₂	1.0 M H ₂ SO ₄	520 mV	13
Co ₃ O ₄ @C	0.5 M H ₂ SO ₄	370 mV	14
Ag-Co ₃ O ₄ -1	0.5 M H ₂ SO ₄	680 mV	15
Ag-Co ₃ O ₄ -2	0.5 M H ₂ SO ₄	470 mV	16
c-Fe ₂ O ₃	0.5 M H ₂ SO ₄	650 mV	17
Co _{0.05} Fe _{0.95} O _y	0.5 M H ₂ SO ₄	650 mV	18
F-(Mn _{1-x} Nb _x)O ₂	1.0 M H ₂ SO ₄	680 mV	19

References

1. T. Zhao, D. Zhong, G. Hao and Q. Zhao, *Appl. Surf. Sci.*, 2023, **607**, 155079.
2. H. Liu, Z. Zhang, J. Fang, M. Li, M. G. Sendeku, X. Wang, H. Wu, Y. Li, J. Ge and Z. Zhuang, *Joule*, 2023, **7**, 558-573.
3. L. Chong, G. Gao, J. Wen, H. Li, H. Xu, Z. Green, J. D. Sugar, A. J. Kropf, W. Xu, X. M. Lin, H. Xu, L. W. Wang and D. J. Liu, *Science*, 2023, **380**, 609-616.
4. J. Huang, H. Sheng, R. D. Ross, J. Han, X. Wang, B. Song and S. Jin, *Nat. Commun.*, 2021, **12**, 3036.
5. F. Shang, H. He, P. Li, H. Cai, B. An, X. Li, S. Yang, Z. Sun and B. Wang, *J. Colloid Interface Sci.*, 2023, **641**, 329-337.
6. J. S. Mondschein, J. F. Callejas, C. G. Read, J. Y. C. Chen, C. F. Holder, C. K. Badding and R. E. Schaak, *Chem. Mater.*, 2017, **29**, 950-957.
7. J. S. Mondschein, K. Kumar, C. F. Holder, K. Seth, H. Kim and R. E. Schaak, *Inorg. Chem.*, 2018, **57**, 6010-6015.
8. I. A. Moreno-Hernandez, C. A. MacFarland, C. G. Read, K. M. Papadantonakis, B. S. Brunschwig and N. S. Lewis, *Energy Environ. Sci.*, 2017, **10**, 2103-2108.
9. F. Hu, S. Zhu, S. Chen, Y. Li, L. Ma, T. Wu, Y. Zhang, C. Wang, C. Liu, X. Yang, L. Song, X. Yang and Y. Xiong, *Adv. Mater.*, 2017, **29**, 1606570.
10. C. Lei, H. Chen, J. Cao, J. Yang, M. Qiu, Y. Xia, C. Yuan, B. Yang, Z. Li, X. Zhang, L. Lei, J. Abbott, Y. Zhong, X. Xia, G. Wu, Q. He and Y. Hou, *Adv. Energy Mater.*, 2018, **8**, 1801912.

11. M. Musiani, *Chem. Commun.*, 1996, **21**, 2403-2404.
12. P. P. Patel, M. K. Datta, O. I. Velikokhatnyi, R. Kuruba, K. Damodaran, P. Jampani, B. Gattu, P. M. Shanthi, S. S. Damle and P. N. Kumta, *Sci. Rep.*, 2016, **6**, 28367.
13. L. Zhou, A. Shinde, J. H. Montoya, A. Singh, S. Gul, J. Yano, Y. Ye, E. J. Crumlin, M. H. Richter, J. K. Cooper, H. S. Stein, J. A. Haber, K. A. Persson and J. M. Gregoire, *ACS Catal.*, 2018, **8**, 10938-10948.
14. X. Yang, H. Li, A. Y. Lu, S. Min, Z. Idriss, M. N. Hedhili, K. W. Huang, H. Idriss and L. J. Li, *Nano Energy*, 2016, **25**, 42-50.
15. K. L. Yan, J. Q. Chi, J. Y. Xie, B. Dong, Z. Z. Liu, W. K. Gao, J. H. Lin, Y. M. Chai and C. G. Liu, *Renew. Energy*, 2018, **119**, 54-61.
16. K. L. Yan, J. F. Qin, J. H. Lin, B. Dong, J. Q. Chi, Z. Z. Liu, F. N. Dai, Y. M. Chai and C. G. Liu, *J. Mater. Chem. A*, 2018, **6**, 5678-5686.
17. W. L. Kwong, C. C. Lee, A. Shchukarev, E. Björn and J. Messinger, *J. Catal.*, 2018, **365**, 29-35.
18. W. L. Kwong, C. C. Lee, A. Shchukarev and J. Messinger, *Chem. Commun.*, 2019, **55**, 5017-5020.
19. S. D. Ghadge, O. I. Velikokhatnyi, M. K. Datta, P. M. Shanthi, S. Tan and P. N. Kumta, *ACS Appl. Energy Mater.*, 2020, **3**, 541-557.